Electronic Supplementary Information (ESI)

Enhancing the photocatalytic activity of BiOX (X = Cl, Br, I), $(BiO)_2CO_3$ and Bi_2O_3 by modifying their surfaces with polar organic anions, 4-substituted thiophenolates

Benyan Xu[a], Yang An[a], Yuanyuan Liu[*a], Xiaoyan Qin[a], Xiaoyang Zhang[a], Ying Dai[b], Zeyan Wang[a], Peng Wang[a], Myung-Hwan Whangbo[a,c] and Baibiao Huang[*a]

a. State Key Laboratory of Crystal Materials, Shandong University, Shandong 250100, P. R. China.

E-mail: yyliu@sdu.edu.cn, bbhuang@sdu.edu.cn. Tel: +86-531-8836-6324.

b. School of Physics, Shandong University, Shandong 250100, P. R. China.

c. Department of Chemistry, North Carolina State University, Raleigh, NC 27695-8204, USA.

[1] Synthesis

All reagents used in our experiments are of analytical grade and used directly without further purification.

1. Synthesis of BiOCl and 4CBT@BiOCl

1.1. BiOCl with different facets

BiOCl samples terminated with {001} and {010} facets were synthesized by a hydrothermal procedure. 5 mmol of $Bi(NO_3)_3 \cdot 5H_2O$ and 5 mmol of KCl were added in 70 mL distilled water at room temperature with continuous stirring. Then the pH value was adjusted to 1 or 6 by adding NaOH solution before transferred into a 100 mL Teflon-lined stainless autoclave. The autoclave was kept at 160 ^{o}C for 24 h, and then cooled to room temperature naturally. The obtained products were collected, washed with deionized water and ethanol three times, and dried at 60 ^{o}C for 12 h. The BiOCl obtained under pH = 1 has the {001} facet exposed, while the BiOCl obtained under pH = 6 has the {010} facet exposed. Using the same synthetic process as used for BiOCl under pH = 6, BiOBr and BiOI were synthesized by adding KBr and KI, respectively, instead of KCl.

1.2. BiOCl with different sizes

BiOCl samples with different thickness were synthesized by a hydrothermal procedure. 5 mmol of $Bi(NO_3)_3 \cdot 5H_2O$, 5 mmol of KCl and 0.05 ghexadecyl trimethyl ammonium bromide (CTAB) were added in 70 mL distilled water at room temperature with continuous stirring.

Then the pH value was adjusted to 6 by adding NaOH solution before transferred into a 100 mL Teflon-lined stainless autoclave. The autoclave was kept at 160 ^{o}C for 24 h or 48 h. Changing the reaction time is to control the thickness of the particles. Then the obtained products were collected, washed with deionized water and ethanol three times, and dried at 60 ^{o}C for 12 h. The obtained BiOCl nanosheets at 160 ^{o}C for 24 h and 48 h are about 210 nm and 300 nm in size, and denoted as $BiOCl_{(210\ nm)}$ and $BiOCl_{(300\ nm)}$, respectively, .

4CBT@BiOCl with different facets and sizes were synthesized by a hydrothermal procedure. In a typical procedure, 0.67 mmol BiOCl and 1.33 mmol 4CBT-H were dispersed in 60 mL of deionized water. Subsequently, 20 mL of N,N-Dimethylformamide (DMF) was added into the above suspension. After stirring for 30 min, the obtained suspension was transferred into a 100 mL Teflon-lined stainless autoclave and kept at 120 ^{o}C for 24 h, and then cooled to room temperature naturally. The product was collected, washed with deionized water and absolute ethanol for three times, and dried at 60 ^{o}C for 12 h.

4-substituted thiophenolates 4-Z-$C_6H_4S^-$ (Z = NO_2, H, CH_3, NH_2) were introduced into BiOX (X = Cl, Br, and I). The synthesis pathways were similar to that for 4CBT@BiOCl. The only difference is that a lower temperature was used for 4-NH_2-C_6H_4SH, which was prepared at 90 ^{o}C for 24 h.

2. Synthesis of $(BiO)_2CO_3$ and 4CBT@$(BiO)_2CO_3$

2.1. $(BiO)_2CO_3$with different facets

$(BiO)_2CO_3$ with dominantly exposed {013} and {001} facets were synthesized using the

hydrothermal method previously reported.[1] In a typical synthesis of $(BiO)_2CO_3$ with dominantly exposed {013} facets, 2 mmol bismuth citrate and 2 mmol of urea were dissolved in 70 mL deionized water with continuous stirring. After that, the suspension was transferred into 100 mL Teflon-lined stainless autoclave. The autoclave was kept at 180 ^oC for 24 h. The obtained product was collected, washed with deionized water and absolute ethanol for three times, and dried at 60 ^oC for 12 h.

In a typical synthesis of $(BiO)_2CO_3$ with dominantly exposed {001} facet, 2 mmol $Bi(NO_3)_3 \cdot 5H_2O$ and 6 mmol of urea were dissolved in 70 mL deionized water with continuous stirring. After that, the suspension was transferred into 100 mL Teflon-lined stainless autoclave. The autoclave was kept at 180 ^oC for 24 h. The obtained product was collected, washed with deionized water and absolute ethanol for three times, and dried at 60 ^oC for 12 h.

2.2. $(BiO)_2CO_3$ with different sizes

$(BiO)_2CO_3$ with different sizes were prepared by a hydrothermal method. In a typical procedure, 1.67 mmol urea and 10 mmol $Bi(NO_3)_3 \cdot 5H_2O$ were added into 80 ml water. After being magnetically stirred at room temperature for 0.5 h, the resulting suspension was transferred into a 100 mL a Teflon-lined autoclave and kept at 200 ^oC for 16 h and 48 h, respectively. The reactors were cooled to room temperature naturally. The resulting products $(BiO)_2CO_3$ were collected, washed with distilled water and then dried at 60 ^oC for 12 h. 4CBT@$(BiO)_2CO_3$ was synthesized using the procedure similar to that employed for

4CBT@BiOCl.

3. Synthesis of α- and β-Bi_2O_3 and 4CBT@Bi_2O_3

α- and β-Bi_2O_3 phases were synthesized using a precipitation method. Firstly, 2 g $Bi(NO_3)_3 \cdot 5H_2O$ was dissolved in 20 mL of 1 mol·L^{-1} aqueous nitric acid solution and stirred for 10 minutes to get a clear solution. Then 0.1 g CTAB was added into the solution and stirred for another 20 minutes, labelled as solution A. Subsequently, 200 mL 2 mol·L^{-1} aqueous NaOH solution was introduced into solution A and ultrasonically vibrated for 20 minutes. The precursor powder was collected, washed and dried at 80 ^{o}C for 12 h, and then heat treated in the muffle furnace in the air at 500 ^{o}C for 2 h to obtain α-Bi_2O_3 phase. Meanwhile, solution B was also prepared in the same way as solution A. Then 0.4 g oxalic acid was added into solution B and stirred for 30 minutes. After ultrasonic dispersing for 10 minutes, the precursor was collected, washed and dried at 80 ^{o}C for 12 h. Calcination of the precursor powder at 270 ^{o}C for 2 h yielded β-Bi_2O_3 phase.

4CBT@Bi_2O_3 was prepared in a way similar to that employed for 4CBT@BiOCl.

4. Synthesis of 4CBT-Bi^{3+} complex

For comparison, a complex of Bi^{3+} ion with 4CBT was prepared by a hydrothermal method. 1.5 mmol $Bi(NO_3)_3 \cdot 5H_2O$ and 1.5 mmol 4CBT-H were dispersed in 60 mL of deionized water. After stirring for 30 min, the obtained suspension was transferred into a 100 mL Teflon-lined stainless autoclave and kept at 120 ^{o}C for 24 h, and then cooled to room

temperature naturally. The product was collected, washed with deionized water and absolute ethanol for three times, and dried at 60 ^{o}C for 12 h.

5. Synthesis of 4CBT@Bi_2S_3

4CBT@Bi_2S_3 was prepared by a deposition-precipitation method. Because the molar ratio of 4CBT to Bi in 4CBT@BiOCl measured from the EDS measurements is about 12%, 4CBT@Bi_2S_3 with the same ratio is prepared for comparison. In a typical synthetic route, 2.1 mmol of $Bi(NO_3)_3{\cdot}5H_2O$ was dissolved in 60 mL of ethylene glycol solution. Then 3.1 mmol of Na_2S was added to the $Bi(NO_3)_3$ solution with stirring. After a period of time, 0.25 mmol of 4CBT-H was added to the above solution with constant stirring. Subsequently, the resulting suspension was then kept at 80 ^{o}C with stirring for 6 h. Finally, the precipitates 4CBT@Bi_2S_3 with ~12% of molar percentage ratio of 4CBT to Bi were collected, washed and dried at 60 ^{o}C in air. For comparison, pure Bi_2S_3 was also synthesized without 4CBT-H.

6. Synthesis of other common photocatalysts

g-C_3N_4 was synthesized using a calcination method. Melamine was calcined in a tube furnace (GSL-1100X, Hefei KJ Group) at 500 ^{o}C for 4 h in air to obtain g-C_3N_4. N-doped P25 was synthesized by calcining P25 at 500 ^{o}C for 10 h in nitrogen.

WO_3 was prepared by heating H_2WO_4 at 300 ^{o}C for 1h. To obtain yellow H_2WO_4, a certain amount of sodium tungstate dihydrate ($Na_2WO_4{\cdot}2H_2O$) was dissolved into ethanol-water solution (1:2, v/v). Then the pH of the Na_2WO_4 solution was adjusted to 2.0 by dilute HNO_3 solution (0.1 mol/L) at 60 ^{o}C. After being stirring for 6 h, H_2WO_4 precipitate was

collected.

Cu_2O was synthesized using a precipitation method. Certain stoichiometric amounts of copper sulfate pentahydrate ($CuSO_4 \cdot 5H_2O$) and NaOH were added into 100 mL water and stirred for 30 min to obtain a light blue $Cu(OH)_2$ suspension. Then, 50 mL ascorbic acid was added into the $Cu(OH)_2$ suspension quickly. After stirring for 30 min, the light blue suspension changed to orange suspension. The resulting product was collected, washed and dried at 60 ^{o}C for 12 h in vacuum oven to obtain Cu_2O.

[2] Characterization

1. Structure and property

The crystalline structures of the products were examined by XRD analysis at room temperature on a Bruker AXS D8 advanced X-ray powder diffractometer with Cu Kα radiation (λ= 1.54056 Å). The morphologies of the samples were determined by SEM (Hitachi S-4800 microscope) and high-revolution transmission electron microscope (HRTEM) (JEOL JEM-2100). The Brunauer–Emmett–Teller (BET) surface areas of the samples were measured by a Micromeritics ASAP2020 analyzer at liquid nitrogen temperature. UV-visible DRS analysis was carried out using a Shimadzu UV 2550 recording spectrophotometer, which was equipped with an integrating sphere and $BaSO_4$ was used as a reference. XPS analysis was carried out on a Thermo Fisher Scientific Escalab 250 spectrometer and C 1s (284.6 eV) was used to calibrate the peak positions. Fourier transform infrared (FT-IR) spectra were evaluated by the FT-IR spectrometer (Nicolet Nexus 670). The time-resolved fluorescence spectra were obtained on Edinburgh FLS920 PL. The decay curve

was fitted by using a biexponential decay function to deconvolute the instrument response function. The average lifetime was calculated by using the following relation: $\langle\tau_{av}\rangle = a_1\tau_1 + a_2\tau_2$, ($\tau_1$ and τ_2 are the lifetime, a_1 and a_2 are normalized pre-exponential factors), The excitation source is a 377.8 nm laser. The second harmonic generation (SHG) signal from the sample was selectively detected by a photomultiplier tube (PMTH-S1V1-CR131), averaged by a fast-gated integrator and boxcar averager (Stanford Research Systems), and then recorded by data acquisition software. All experiments were performed at room temperature.

2. Zeta potentials

The Zeta potentials of the photocatalysts were investigated, and the results are summarized in **Table S1**, which shows that the Zeta potentials of BiOCl, $(BiO)_2CO_3$ and Bi_2O_3 are more negative after the surface modification of polar 4CBTs. These results support our conclusion that 4CBT modification of these Bi-based semiconductors creates a polar surface at the interface.

Table S1. Zeta potential (mV) of various photocatalysts

$BiOCl_{\{001\}}$	4CBT@$BiOCl_{\{001\}}$	$BiOCl_{\{010\}}$	4CBT@$BiOCl_{\{010\}}$	4CBT-H
-28.1	-32.6	-26	-34.2	-10.5

$BOC_{(100nm)}$	4CBT@$BOC_{(100nm)}$	$BOC_{(200nm)}$	4CBT@$BOC_{(200nm)}$	4CBT-H
-24	-29.7	-22.3	-31	-10.5

α-Bi_2O_3	4CBT@α-Bi_2O_3	β-Bi_2O_3	4CBT@β-Bi_2O_3	4CBT-H
-27.5	-29.1	-19.4	-28.7	-10.5

3. Photocatalytic properties

The photocatalytic performance of the as-prepared products was evaluated by rhodamine-B (RhB) and methylene blue (MB) degradation at room temperature. In a typical process, 50 mg catalyst was dispersed in 100 mL RhB (or MB) solution (20 mg L^{-1}) and stirred magnetically for 1-2 h in the dark to establish an adsorption-desorption equilibrium. The concentration of catalyst-free RhB solution collected at irradiation time intervals was analyzed on a UV-vis spectrophotometer (Shimadzu UV 2550) with deionized water as a reference sample.

Photocatalytic oxygen evolution reaction was carried out in a top-irradiation vessel connected to a glass-enclosed gas circulation system. In a typical procedure, 50 mg of catalyst was suspended in 50mL aqueous solution containing 50 mg $AgNO_3$ with constant stirring. The reaction temperature was maintained at 5 ^{o}C. The amount of O_2 evolved was determined by using a gas chromatograph (Techcomp GC7890Ⅱ).

The source for UV-Vis light was a 300W Xe arc lamp. The visible light ($\lambda \geq 420$ nm) was obtained using a UV-cutoff filter. The ultraviolet light source is a 10W H-UV lamp with two wavelengths (185 and 254 nm).

4. Electrochemical measurements

The electrochemical measurements were carried out using a 263A Princeton Applied Research (PAR) potentialstat/galvanostat. The photocurrents were measured by an electrochemical analyzer in a standard three-electrode system, with the catalyst-coated FTO glass as the working electrode, a Pt foil as a counter electrode, and a saturated Ag-AgCl

electrode (saturated KCl) as the reference electrode. The light source was a 300W Xe arc lamp. The electrolyte was 0.1M LiCl acetonitrile solution.

5. Calculations of the rate constant for photocatalytic degradation reactions:

The results of photodegradation reactions can be summarized by determining the apparent rate constants, k_{app}, which is describe in terms of the apparent pseudo-first-order kinetics equation (1) [2,3]

$$\ln\frac{C}{C_0} = -k_{app}t \qquad (1)$$

where k_{app} is the rate constant (min^{-1}), C is the concentration ($mg \cdot L^{-1}$) of RhB in aqueous solution at time t, and C_0 is the initial concentration of RhB at t = 0.

6. 4CBT@BiOCl: Facet-dependent activity

SEM images reveal that $BiOCl_{\{010\}}$ is composed of nanosheets with width of 1~3 μm and thickness of 220~300 nm (**Fig. S1a, b**). The SAED pattern from TEM of $BiOCl_{\{010\}}$ displays (200) and (111) planes, which can be indexed as the [010] zone of tetragonal BiOCl (**Fig. S1c**). $BiOCl_{\{001\}}$ consists of nanosheets with width of 2~3.5 μm and thickness of 350~400 nm (**Fig. S1d, e**). SAED patterns from TEM of $BiOCl_{\{001\}}$ displays (102) and (002) planes, which can be indexed as the [001] zone of tetragonal BiOCl (**Fig. S1f**).

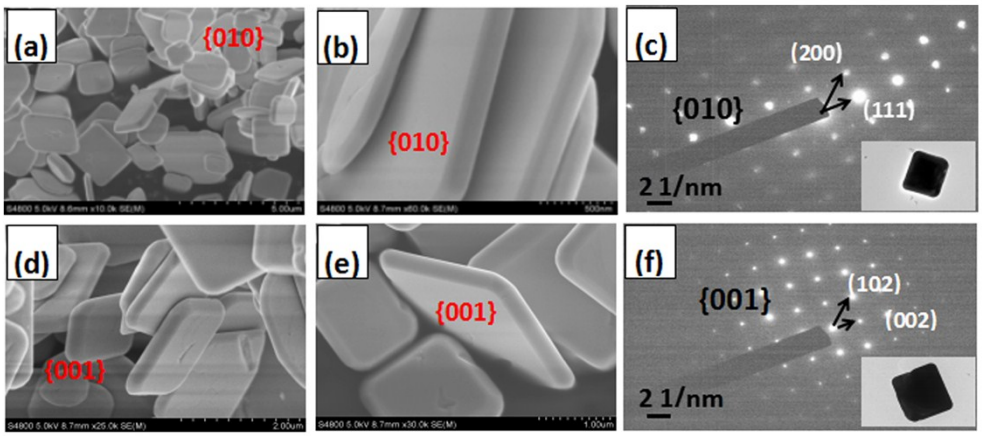

Fig. S1 (a, b) SEM images of $BiOCl_{\{010\}}$, and (c) the corresponding SAED pattern of $BiOCl_{\{010\}}$ (the inset is TEM image). (d, e) SEM images of $BiOCl_{\{001\}}$, and (f) the corresponding SAED pattern of $BiOCl_{\{001\}}$ (the inset is TEM image).

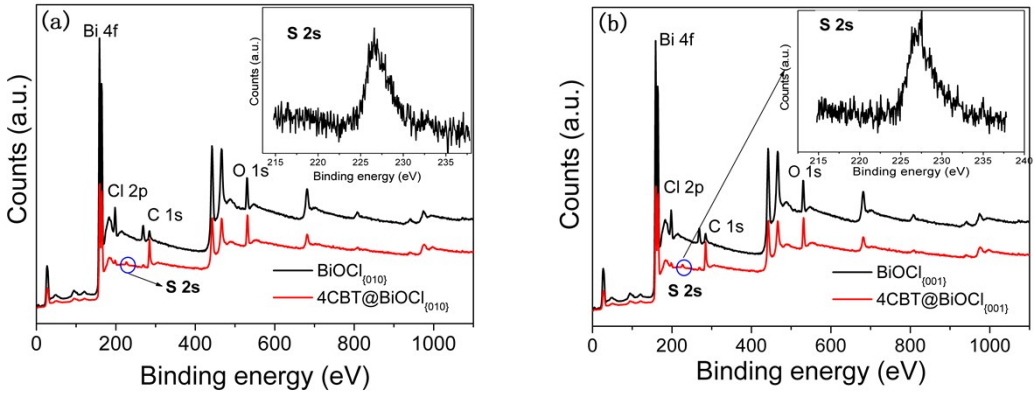

Fig. S2 XPS survey spectra of (a) $BiOCl_{\{010\}}$ and 4CBT@$BiOCl_{\{010\}}$, and those of (b) $BiOCl_{\{001\}}$ and 4CBT@$BiOCl_{\{001\}}$.

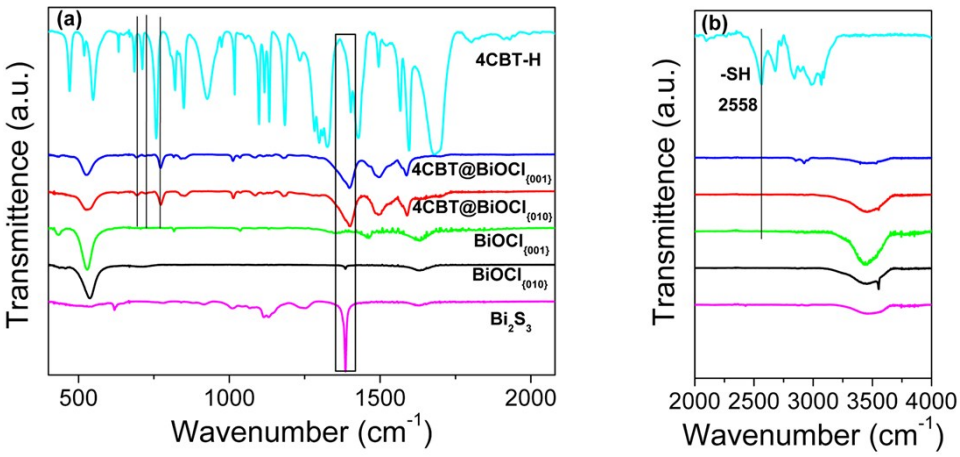

Fig. S3 FT-IR spectra of different samples in the wavenumber regions of (a) 400 ~ 2000 cm^{-1} and (b) 2000~4000 cm^{-1}.

In **Fig. S3**, both 4CBT@BiOCl$_{\{001\}}$ and 4CBT@BiOCl$_{\{010\}}$ have the same peaks, while they display some typical peaks of BiOCl and 4CBT, in good agreement with the reported results[4-9]. However, compared with the FT-IR spectrum of 4CBT, the three characteristic peaks of 4CBT@BiOCl, namely, the ν(C-S) stretching vibrational peak at 685 cm^{-1}, the ω(CO2) bending vibrational peak at 711 cm^{-1}, and ν(C-ph) vibrational peak at 758 cm^{-1}, shift respectively ~8.1, ~9.8, and ~15 cm^{-1} towards a higher wavenumber in the spectra of 4CBT@BiOCl. The characteristic δ(SH) peak at ~2558 cm^{-1} disappears because of the deprotonation. Moreover, the spectra of 4CBT@BiOCl exhibit a broad peak region (1331.7~1416.2 cm^{-1}), in which the typical peak of Bi_2S_3 at ~1385 cm^{-1} and the peak of 4CBT at 1401.9 cm^{-1} overlap. In addition, the stretching vibration peak of Bi-O bond (527 cm^{-1}) in 4CBT@BiOCl becomes weaker than that in BiOCl. All the above changes are mainly due to the formation of Bi-S bonds.

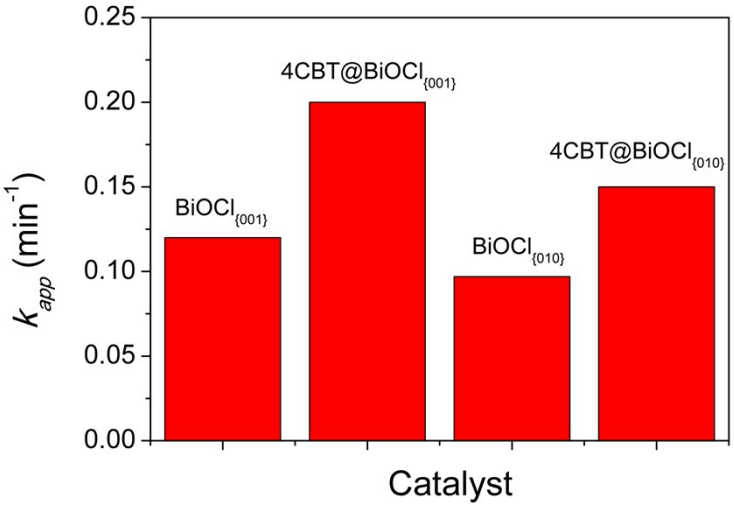

Fig. S4 The values of the apparent rate constant k_{app} for the photocatalytic degradation of RhB under UV light irradiation over BiOCl$_{\{001\}}$, BiOCl$_{\{010\}}$, 4CBT@BiOCl$_{\{001\}}$ and 4CBT@BiOCl$_{\{010\}}$.

7. 4CBT@$(BiO)_2CO_3$ nanosheets: Size-dependent activity

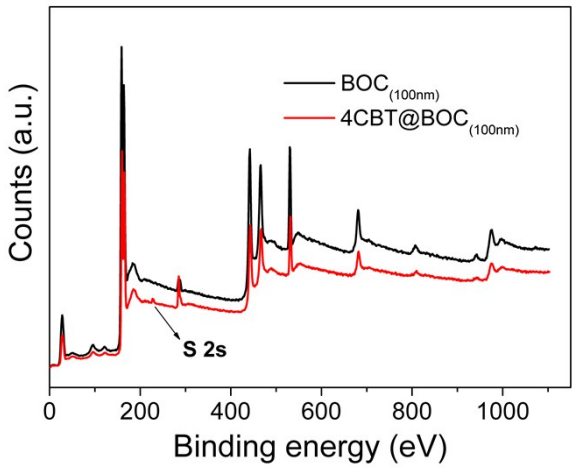

Fig. S5 XPS survey spectra of 4CBT@$BOC_{(100nm)}$ and $BOC_{(100nm)}$.

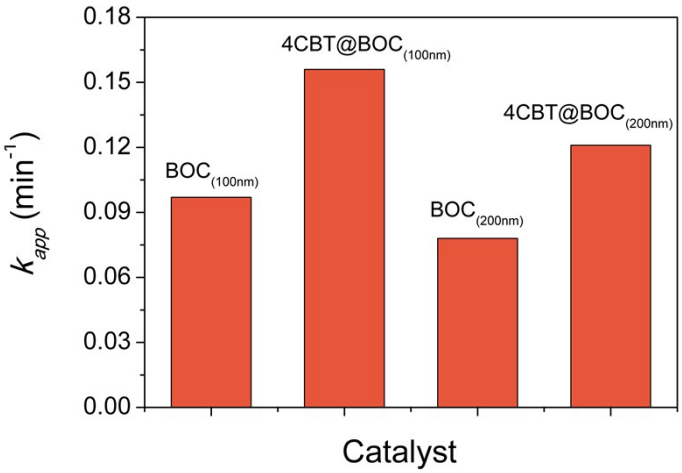

Fig. S6 The values of the apparent rate constant k_{app} for RhB photocatalytic degradation process under UV light irradiation over $BOC_{(100nm)}$, $BOC_{(200nm)}$, 4CBT@$BOC_{(100nm)}$ and 4CBT@$BOC_{(200nm)}$.

8. 4CBT@Bi_2O_3: Phase-dependent activity

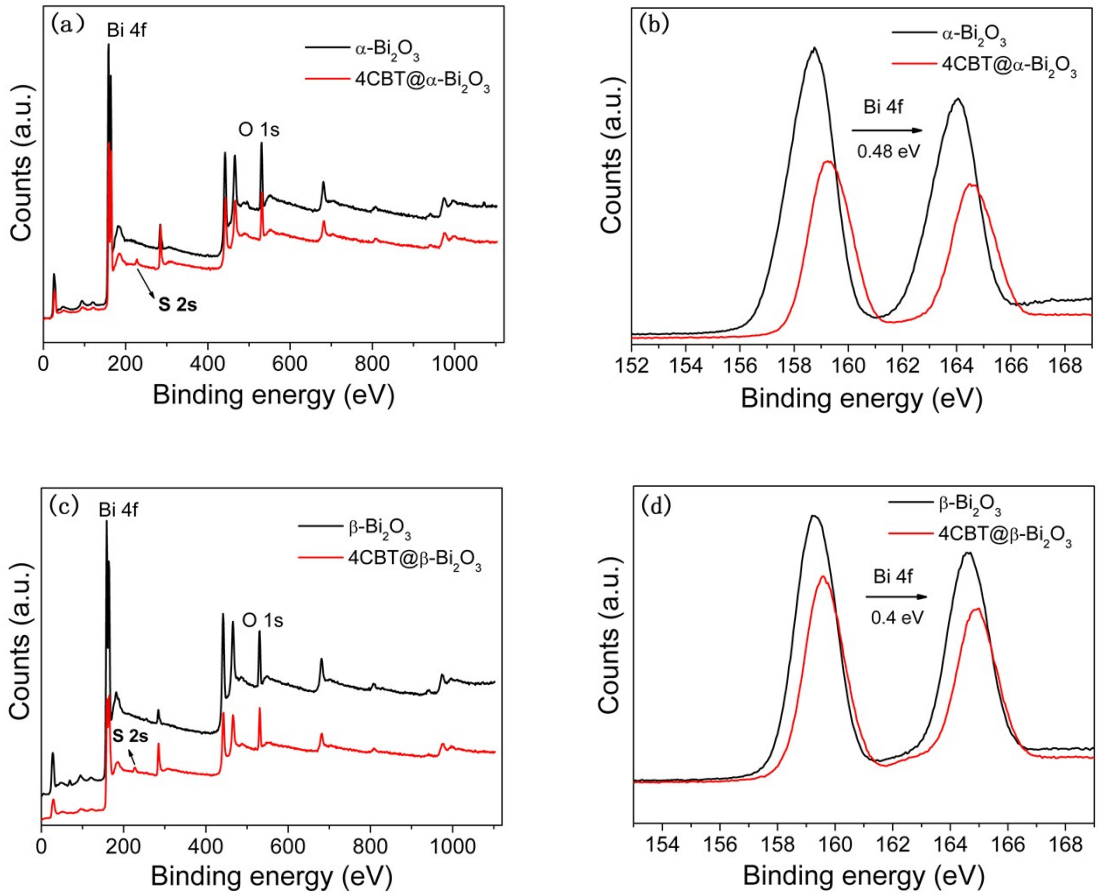

Fig. S7 (a, b) XPS spectra of the Bi 4f state of 4CBT@α-Bi_2O_3 and α-Bi_2O_3; (c, d) XPS spectra of 4CBT@β-Bi_2O_3 and β-Bi_2O_3.

XPS analysis was carried out to confirm the existence of Bi-S bonds formed between Bi_2O_3 and 4CBT. In the survey spectra of 4CBT@α-Bi_2O_3 (**Fig. S7a**) and 4CBT@β-Bi_2O_3 (**Fig. S7c**), Bi, O and S elements are detected, respectively. The binding energy located at 227.3 eV is assigned to the S 2s state. More importantly, the Bi 4f states of 4CBT@α-Bi_2O_3 obviously shift about 0.48 eV towards a higher binding energy with respect to that of α-Bi_2O_3 (**Fig. S7b**), while the Bi 4f states of 4CBT@β-Bi_2O_3 have a shift of 0.4 eV towards a higher

binding energy compared with that of β-Bi_2O_3 (**Fig. S7d**). These shifts are due to the formation of Bi-S bonds. However, these results are different from those found for 4CBT@BiOCl and 4CBT@$(BiO)_2CO_3$ because, in the latter, the Bi 4f states shift towards a lower binding energy. The shift of the Bi 4f states in different directions may arise from the fact that the Bi-O bond energy in Bi_2O_3 (342.3kJ/mol)[10] is stronger than that of the $Bi_2O_2^{2+}$ slabs in BiOCl (337.2 kJ/mol).[11] This difference might give rise to different electron distributions around Bi^{3+} ions in the O-Bi-S bonds after the surface-modification with 4CBT on Bi_2O_3 and BiOCl.

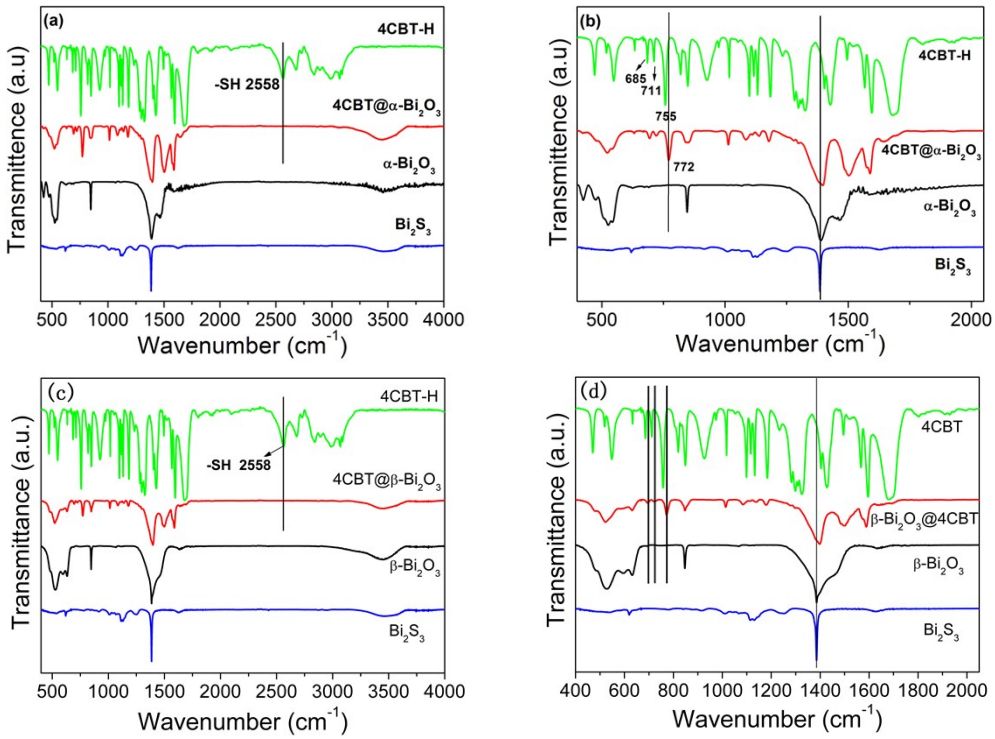

Fig. S8 (a, b) FT-IR spectra of 4CBT@α-Bi_2O_3 and α-Bi_2O_3. (c, d) FT-IR spectra of 4CBT@β-Bi_2O_3 and β-Bi_2O_3.

FT-IR spectra also verify the presence of Bi-S bonds, as shown in **Fig. S8**. The results are similar to those obtained for 4CBT@BiOCl. 4CBT@α-Bi_2O_3 and 4CBT@β-Bi_2O_3 consist of the typical peaks observed for α- and β-Bi_2O_3[12] and 4CBT-H.[6-9] Compared with the FT-IR spectrum of 4CBT-H, the characteristic δ(SH) peak at about 2558 cm^{-1} disappears (**Fig. S8a**). The three characteristic peaks of 4CBT@α-Bi_2O_3, namely, the ν(C-S) stretching vibrational peak at 685 cm^{-1}, the ω(CO2) bending vibrational peak at 711 cm^{-1}, and ν(C-ph) vibrational peak at 755 cm^{-1}, shift respectively about 8.1, 9.8, and 15 cm^{-1} towards a higher wavenumber (**Fig. S8b**). Moreover, the band at 1389 cm^{-1} assigned to the ν(Bi-O) stretching vibrational peak in α-Bi_2O_3 shifts to 1399 cm^{-1} in 4CBT@α-Bi_2O_3. The above changes are due mainly to the formation of Bi-S bonds in 4CBT@α-Bi_2O_3. In the broad peak region (1318~1429 cm^{-1}) of 4CBT@α-Bi_2O_3, the typical peak of Bi_2S_3 at about 1385 cm^{-1} and the peak of 4CBT at 1402 cm^{-1} overlap. 4CBT@β-Bi_2O_3 exhibits the result similar to those of 4CBT@α-Bi_2O_3 (**Fig. S8c, d**). All the above results demonstrate the formation of Bi-S bonds.

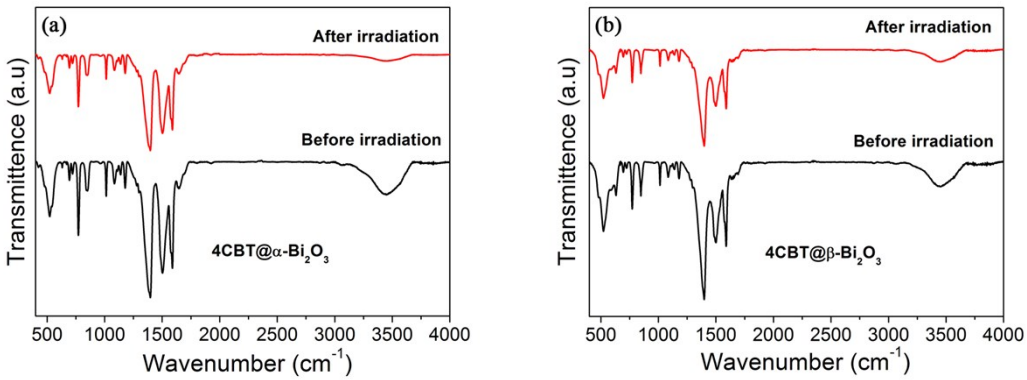

Fig. S9 FT-IR spectra of 4CBT@α-Bi_2O_3 and 4CBT@β-Bi_2O_3 before and after the visible light irradiation (> 8h) for the degradation of RhB.

9. Effect of the Bi-S bond on the light absorption and photocatalytic activity

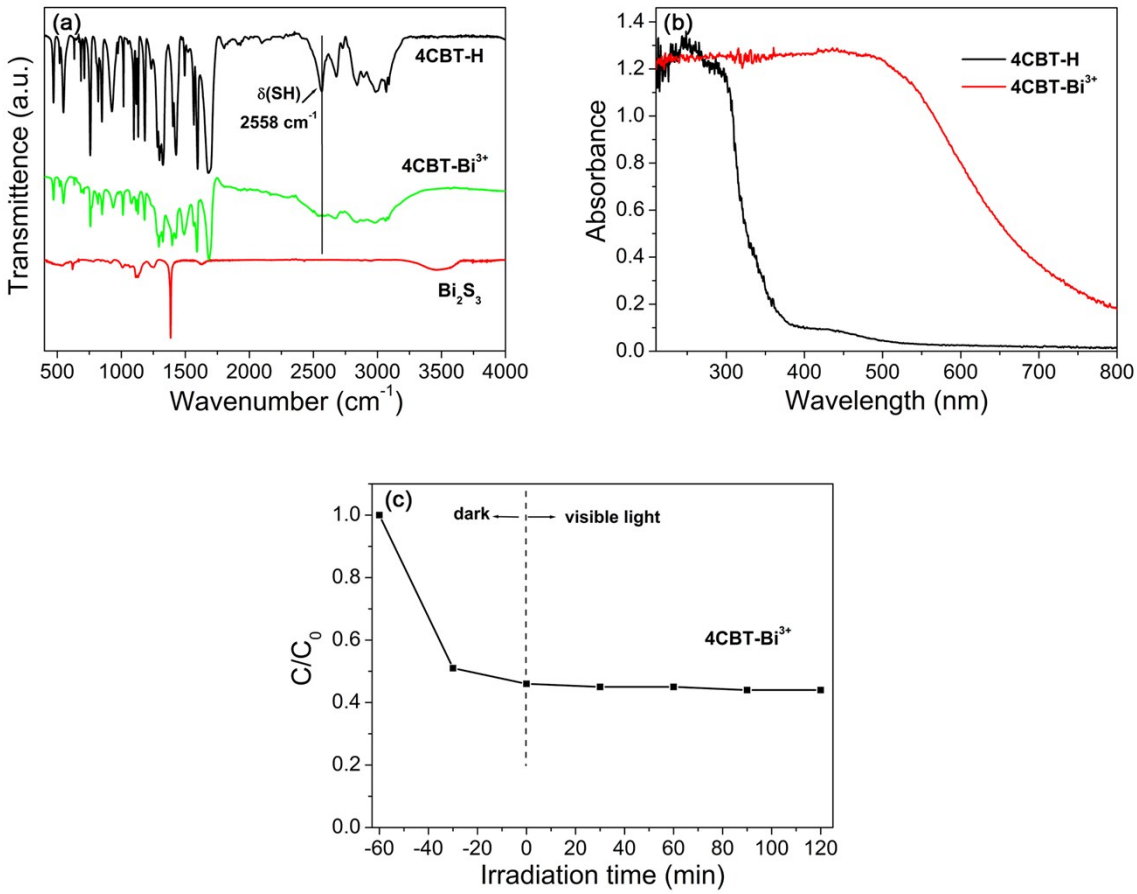

Fig. S10 (a) FT-IR spectra and (b) DRS spectra of the 4CBT-Bi^{3+} complex. (c) Photocatalytic degradation of RhB over the complex of the 4CBT-Bi^{3+} complex under visible light irradiation.

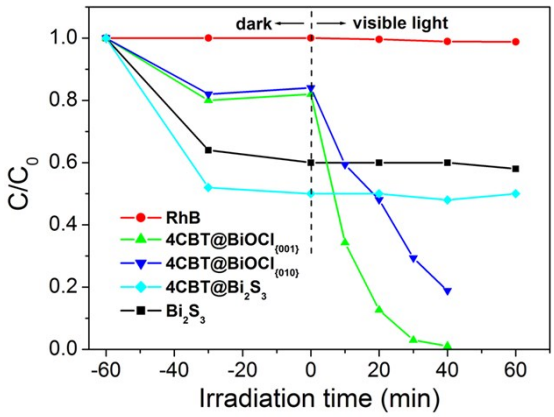

Fig. S11 Photodegradation of RhB over 4CBT@Bi_2S_3 and 4CBT@$BiOCl_{\{001\}}$ under visible light irradiation.

10. Photocatalytic and optical properties of other common photocatalysts

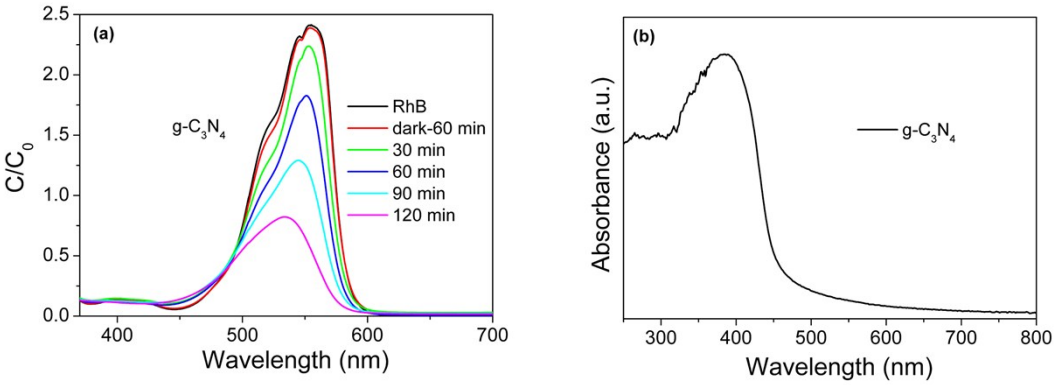

Fig. S12 (a) UV-Vis spectra of a RhB aqueous solution in the presence of g-C_3N_4 under visible light irradiation as a function of the irradiation time. (b) UV-Vis absorption spectra of g-C_3N_4.

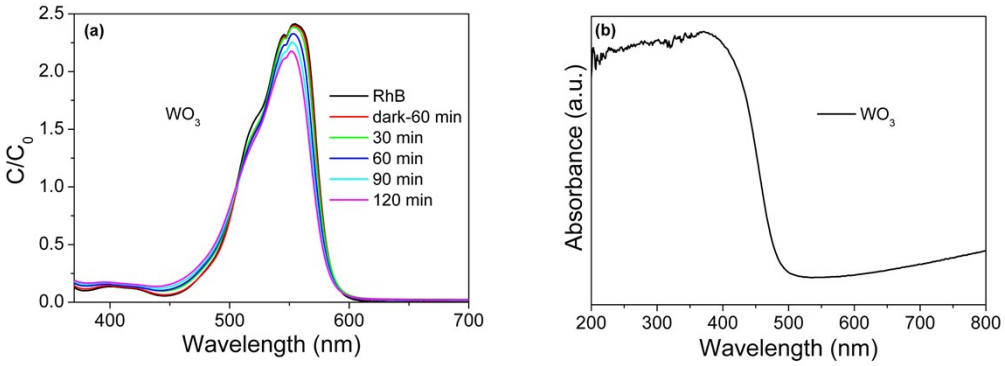

Fig. S13 (a) UV-Vis spectra of a RhB aqueous solution in the presence of WO_3 under visible light irradiation as a function of the irradiation time. (b) UV-Vis absorption spectra of WO_3.

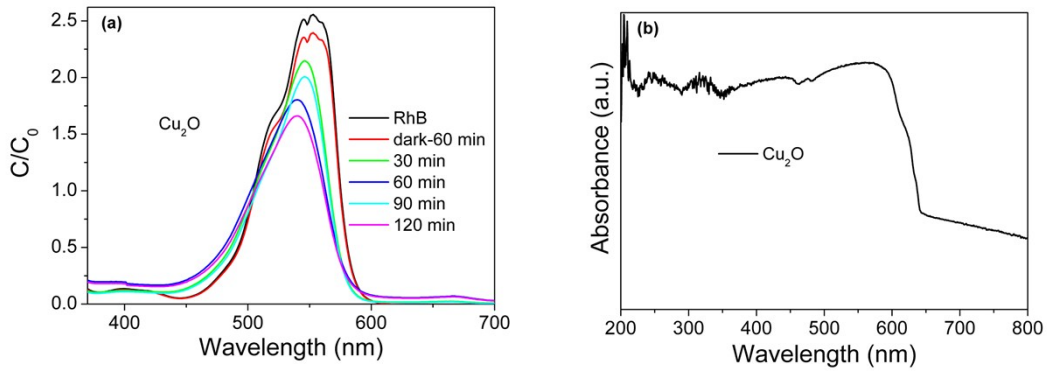

Fig. S14 (a) UV-Vis spectra of a RhB aqueous solution in the presence of Cu_2O under visible light irradiation as a function of the irradiation time. (b) UV-Vis absorption spectra of Cu_2O.

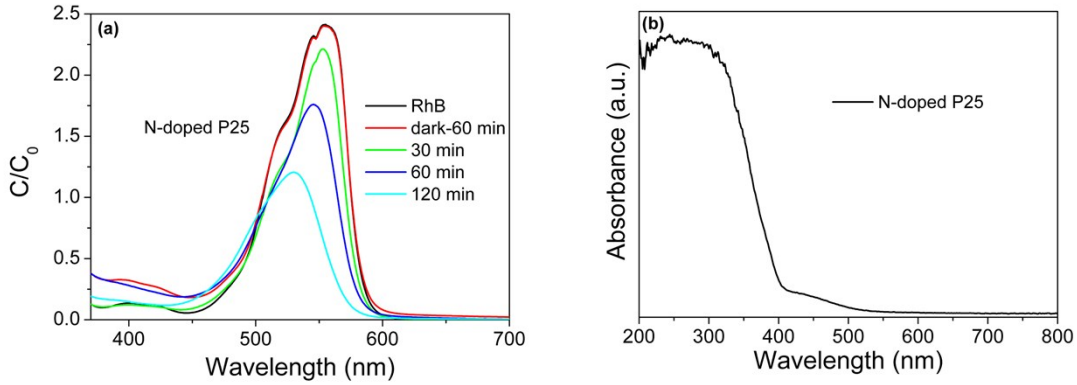

Fig. S15 (a) UV-Vis spectra of a RhB aqueous solution in the presence of N-doped P25 under visible light irradiation as a function of the irradiation time. (b) UV-Vis absorption spectra of N-doped P25.

References

1 H. W. Huang, J. J. Wang, F. Dong, Y. X. Guo, N. Tian, Y.H. Zhang and T. R. Zhang, *Cryst. Growth Des.* 2015, **15**, 534.

2 K. Dai, L. H. Lu, C. H. Liang, Q. Liu and G. P. Zhu, *Appl. Catal. B: Environ.*, 2014, **156-157**, 331.

3 Y. Hong, C. G. Tian, B. J. Jiang, A. P. Wu, Q. Zhang, G. H. Tian and H. G. Fu, *J. Mater. Chem. A*, 2013, **1**, 5700.

4 Q. B. Li, X. Zhao, J. Yang, C. J. Jia, Z. Jin and W. L. Fan, *Nanoscale*, 2015, **7**, 18971.

5 X. Y. Gao, X. C. Zhang, Y. W. Wang, S. Q. Peng, B. Yue and C. M. Fan, *Chem. Eng. J.*, 2015, **263**, 419.

6 Y. Zhou, H. Zhao, C. Li, P. He, W. B. Peng, L. F. Yuan, L. X. Zeng and Y. J. He, *Talanta*, 2012, **97**, 331.

7 R. Li, H. M. Lv, X. L. Zhang, P. P. Liu, L. Chen, J. B. Cheng and B. Zhao, *Spectrochim. Acta, Part A: Mol. Biomol. Spectro.*, 2015, **148**, 369.

8 Y. Zhou, H. Zhao, Y. J. He, N. Ding and Q. Cao, *Colloids Surf., A: Physicochem. Eng. Aspects*, 2011, **391**, 179.

9 P. K. Sudeep, S. T. S. Joseph and K. G. Thomas, *J. Am. Chem. Soc.*, 2005, **127**, 6516.

10 M. Mohsen, E. Gomaa, M. S. Al-Kotb, M. Abdel-Baki and N. Fathy, *J. Non-Cryst. Solids*, 2016, **436**, 1.

11 L. Q. Ye, L. Zan, L. H. Tian and T. Y. Peng, *Chem. Commun.*, 2011, **47**, 6951.

12 Y. H. Yan, Z. X. Zhou, Y. Cheng, L. L. Qiu, C. P. Gao and J. G. Zhou, *J. Alloys Compd.*, 2014, **605**, 102.